Analysis of Catania Flash Flood Case Study by Using Combined Microwave and Infrared Technique

FRANCESCO DI PAOLA, ELISABETTA RICCIARDELLI, DOMENICO CIMINI, FILOMENA ROMANO, MARIASSUNTA VIGGIANO, AND VINCENZO CUOMO

Institute of Methodologies for Environmental Analysis, National Research Council of Italy, Tito Scalo, Italy

(Manuscript received 22 May 2013, in final form 17 March 2014)

ABSTRACT

In this paper, the analysis of an extreme convective event atypical for the winter season, which occurred on 21 February 2013 on the east coast of Sicily and caused a flash flood over Catania, is presented. In just 1 h, more than 50 mm of precipitation was recorded, but it was not forecast by numerical weather prediction (NWP) models and, consequently, no severe weather warnings were sent to the population. The case study proposed is first examined with respect to the synoptic situation and then analyzed by means of two algorithms based on satellite observations: the Cloud Mask Coupling of Statistical and Physical Methods (MACSP) and the Precipitation Evolving Technique (PET), developed at the National Research Council of Italy. Both of the algorithms show their ability in the near-real-time monitoring of convective cell formation and their rapid evolution. As quantitative precipitation forecasts by NWP could fail, especially for atypical convective events like in Catania, tools like MACSP and PET shall be adopted by civil protection centers to monitor the real-time evolution of deep convection events in aid to the severe weather warning service.

1. Introduction

On 21 February 2013, a heavy rainfall event affected southern Italy, causing a flash flood near Catania, on the east coast of Sicily. This event was characterized by extraordinarily intense rainfall over a short period, discharging more than 50 mm between 1500 and 1600 UTC. The arising flood affected the city of Catania and the surrounding region, causing serious damage to the local infrastructure and economy. The consequences of the flash flood were accentuated by the lack of severe weather warning by the Italian Department of Civil Protection (DPC; Bollettino di Vigilanza Meteorologica Nazionale 2013), because the available numerical weather prediction (NWP) models did not produce an adequate quantitative precipitation forecast (QPF).

In fact, even with modern, state-of-the-art NWP models, the instantaneous QPF is challenging (Gaudet and Cotton 1998) because of the high discontinuity and variability in time and space of rainfall. This is especially true in the case of high-precipitation thresholds and rare events, which are particularly difficult to handle for operational forecasting purposes (Meneguzzo et al. 2004). Moreover, the magnitude, location, and time of rainfall depend on how the used NWP model is able to compute the dimension and the evolution of atmospheric systems involved (Wardah et al. 2011). Generally, there are three types of errors in QPF: intensity, localization, and timing of the precipitation event (Habets et al. 2004; Zimmer and Wernli 2011). These depend not only on the synoptic situation but also on processes not explicitly considered in the NWP model, such as condensational processes on subgrid scale; the phase transitions of water between vapor, cloud, and ice; and vertical convective transports of heat and moisture on subgrid scale (Damrath et al. 2000; Shrestha et al. 2013). For these reasons, NWP QPF is still relatively unsatisfactory, especially for small-scale and short-term high-precipitation events (Cuo and Pagano 2011), such as the local–regional convective systems that often occur in the Mediterranean region.

When NWP QPF fails, the convective systems can be monitored by using satellite measurements at infrared (IR), visible (VIS), or microwave (MW) wavelengths. Many studies have been performed using satellite observations for monitoring precipitation in extreme

Corresponding author address: Francesco Di Paola, Institute of Methodologies for Environmental Analysis, National Research Council of Italy, C.da S. Loja, Zona Industriale, 85050 Tito Scalo (PZ), Italy.
E-mail: francesco.dipaola@imaa.cnr.it

DOI: 10.1175/JHM-D-13-092.1

events (Ferraro et al. 2005; Wilcox and Donner 2007; Wardah et al. 2008; Kummerow et al. 2010; Bennartz and Schroeder 2012; Wu et al. 2012; Casella et. al. 2013, Mugnai et al. 2013a,b; Munchak and Skofronick-Jackson 2013). Comprehensive overviews of satellite remote sensing of precipitation and its applications are given by Kidd and Levizzani (2011) and Kucera et al. (2013).

Passive MW (PM) observations from low-Earth-orbiting (LEO) satellites are useful to provide a good estimate of convective precipitation with a high level of accuracy (Kummerow et al. 2001; Chen and Staelin 2003; Surussavadee and Staelin 2008). However, the spatial resolution of PM observations from LEO satellites is low (~10–50 km), and the temporal sampling does not provide good coverage, because the LEO satellite overpasses the same area once or twice a day at midlatitudes (Di Paola and Dietrich 2008; Dietrich et al. 2011; Price et al. 2011). Because of this, MW observations are unsuitable for monitoring extreme events as well as small-scale events characterized by a high temporal variability.

Conversely, the geosynchronous Earth orbit (GEO) satellite IR and VIS observations provide a good spatial resolution (~1–10 km) and a subhourly temporal sampling, thus ensuring a good monitoring of the small-scale events, even if the observation is related more to the overlying cloud layer rather than to the underlying precipitation. In addition, the relationship between cloud top temperature and rain rate was demonstrated many years ago (Negri and Adler 1981; Adler and Mack 1984; Adler et al. 1985). Many techniques based on GEO satellite observations have been developed in order to estimate rain rate (RR) classes or values (Adler and Negri 1988; Wu et al. 1985; Adler et al. 1993; Hsu et al. 1997; Sorooshian et al. 2000), even if these methods generally use statistical approaches and produce estimates with an accuracy more adequate for global-scale rather than local-scale monitoring.

To obtain more accurate RR estimates with high spatial and temporal sampling at the same time, we exploited the ability of MW radiometers on board LEO satellites to observe precipitation combined with the high spatial and temporal sampling of VIS/IR radiometers on board GEO satellites (Kidd et al. 2003, 2007; Joyce et al. 2004, 2007; Marzano et al. 2004; Huffman et al. 2007; Turk and Mehta 2007; Torricella et al. 2007; Kubota et al. 2007; Casella et al. 2012).

In this paper, we show the application of two different methods, both developed at the National Research Council (CNR) of Italy, to monitor the severe storm event that occurred on 21 February 2013 in southern Italy, which is briefly introduced in section 2. Sections 3 and 4 show an overview of the Cloud Mask Coupling of Statistical and Physical Methods (MACSP) algorithm (Ricciardelli et al. 2008) and Precipitation Evolving Technique (PET) algorithm (Di Paola et al. 2012) and their applications to monitor the evolution of convective cells. Finally, section 5 summarizes these analyses and draws the conclusions.

2. Analysis of 21 February 2013 case study over Sicily

On 20 February 2013 a large depression developed over northern Africa, with a warm advection from the Sahara to the Mediterranean region, culminating in extraordinarily intense rainfall in the following days. These severe storms moved northeast across the Ionian Sea and hit southern Italy first, on the afternoon of 21 February, and then subsequently hit Greece the following morning, producing floods and causing extensive damages.

Figure 1 (top left) shows the mean sea level pressure coupled with 500-hPa geopotential at 1200 UTC 20 February, where a low over Algeria and Tunisia, corresponding to a southern flux at a nondivergent level, can be observed. Figure 1 (top right) shows a map of thermal field and wind vectors at the 850-hPa level, where a flux of mild air moves from northern Africa to the Mediterranean Sea with a strong warm advection toward Sicily. Figure 1 (bottom) shows the same maps at 1500 UTC of the next day, when the intense precipitation near the east coast of Sicily had started, causing a flash flood over Catania. When comparing the top and the bottom of Fig. 1, it is possible to point out the easterly movement of the depression from Algeria to the Libyan Sea with warm advection toward the Ionian Sea.

The synoptic analysis at 1500 UTC 21 February 2013 shows that the strong precipitation over Sicily is the result of a warm conveyor belt (WCB), a well-structured flux of warm moist air running in front of a cold front. This is evident in Fig. 2, which shows the red–green–blue (RGB) composition of 0.8, 3.9, and 10.8 μm Spinning Enhanced Visible and Infrared Imager (SEVIRI) channels, where it is possible to observe the low pressure area centered mainly over Greece and the WCB identified by the large cloud system over central and southern Italy. The intense rainfall that affected the east cost of Sicily and the Calabria region was a consequence of the WCB dynamics that are able to generate very intense and rapid prefrontal storms.

3. MACSP application

MACSP is a cloud classification algorithm developed at CNR in the Institute of Methodologies for

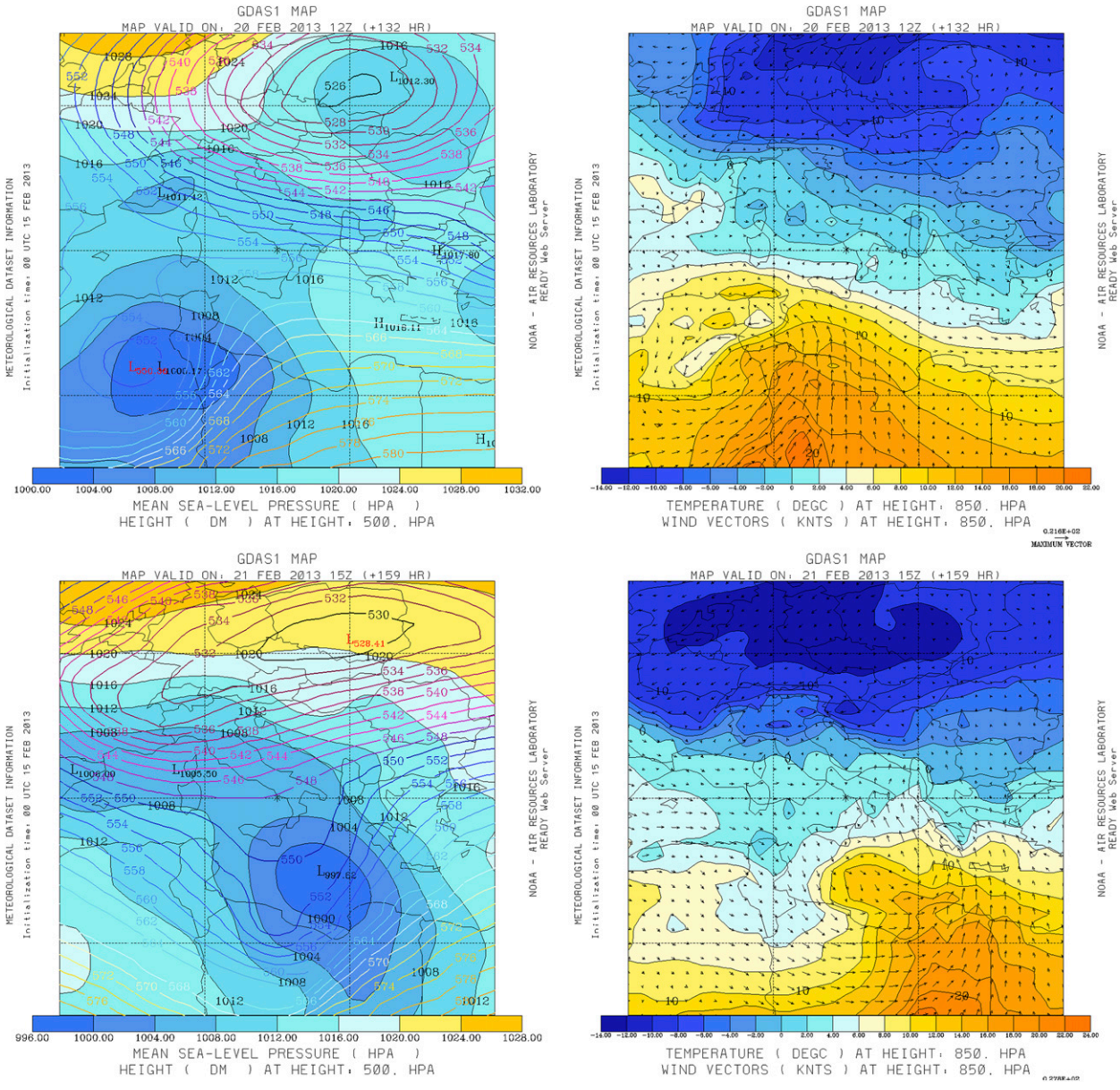

FIG. 1. National Centers for Environmental Prediction (NCEP) Global Data Assimilation System (GDAS) model output (available from NOAA/Air Resources Laboratory). (top left) Mean sea level pressure and 500-hPa-level geopotential at 1200 UTC 20 Feb 2013, (top right) thermal field and wind vector at 850-hPa level at 1200 UTC 20 Feb 2013, (bottom left) mean sea level pressure and 500-hPa-level geopotential at 1500 UTC 21 Feb 2013, and (bottom right) thermal field and wind vector at 850-hPa level at 1500 UTC 21 Feb 2013.

Environmental Analysis (IMAA) to work with observations from the Meteosat Second Generation (MSG) SEVIRI. While earlier versions of MACSP (Ricciardelli et al. 2008) were limited to cloud masking only, giving output flags of "cloudy" or "not cloudy" for each pixel, MACSP was recently updated to provide information about the cloud class as well. A pixel can be classified into six different classes: clear, low cloud, midlevel cloud, high optically thin cloud, high optically thick cloud, and deep convective cloud. The core of the algorithm consists of tests able both to distinguish optically high thin from optically high thick clouds and detect pixels having a high likelihood of deep convection presence.

A new threshold test involving the SEVIRI water vapor (WV) channel considers the difference between the brightness temperatures (BTs) at 6.2- and 10.8-μm channels ($\Delta BT^{6.2\,\mu m-10.8\,\mu m}$), which is useful to detect both midlevel clouds ($\Delta BT^{6.2\,\mu m-10.8\,\mu m}$, in this case the difference is large negative) and deep convective clouds ($\Delta BT^{6.2\,\mu m-10.8\,\mu m}$, in this case the difference is very

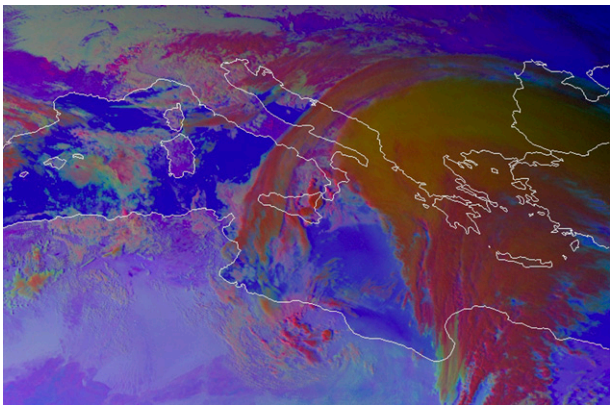

FIG. 2. Day microphysical RGB composition of 0.8, 3.9, and 10.8 μm SEVIRI channels (Lensky and Rosenfeld 2008) at 1500 UTC 21 Feb 2013. The color scheme is useful to detect cumulonimbus (red), optically thick clouds with small ice particles on top (orange), thin clouds with small ice particles (light green), stratocumulus (violet), and water clouds (yellow/green).

small, i.e., close to zero). As a consequence of the new MACSP classes, the algorithm has been trained using a new dataset.

The a priori cloud classification was made through a careful visual analysis of the SEVIRI images. The analysis consists of selecting the cloudy pixels manually after observing the spectral characteristics in IR and VIS images and their RGB composition, which is useful for distinguishing cloud classes (Lensky and Rosenfeld 2008). To test the validity of the MACSP classification algorithm, an independent dataset of ~300 samples gathered for each class has been collected. The dataset was built by selecting images characterized by various cloud types corresponding to the MACSP cloud classes, and it is representative of different weather conditions. A manual classification was made through a careful observation of the SEVIRI images and their RGB composition, and the results were compared with the MACSP cloud classification.

The results of the classification of deep convective clouds were validated by considering as true the radar-derived rain rate values obtained from the Italian Operational Weather Radar Network observations and collected by the Italian DPC. The classification accuracies of the MACSP algorithm are listed in Table 1.

Figure 3 shows the MACSP cloud classification results related to the SEVIRI observations from 1325 to 1710 UTC 21 February 2013. The black pixels indicate convective areas. Two small convective cells are visible in northeastern Sicily between 1325 and 1425 UTC. In the subsequent images, one of these convective cells moves toward the southeast and becomes larger near Catania, as it is possible to observe in the images from 1440 to 1610 UTC. This cell grows and continues to move toward southern Sicily in the subsequent images. Moreover, two convective cells originate in the south of Calabria at 1525 UTC and get larger in the next images. Other convective cells originate in some inner areas of Sicily as well as near the coast.

TABLE 1. Accuracy of the MACSP algorithm on an independent dataset.

Classes	Classification accuracy (%)
Clear	95.0
Low clouds	91.0
Midlevel clouds	92.0
High thin clouds	87.0
High thick clouds	96.0
Convective clouds	94.0

4. PET application

PET is a multisensor algorithm developed by IMAA-CNR and the Institute of Atmospheric Sciences and Climate (ISAC)-CNR, for the continuous monitoring of convective rain cells. This technique is based on RR estimated from PM remote sensing from the National Oceanic and Atmospheric Administration (NOAA) and Meteorological Operation (MetOp) operational LEO satellites coupled with BT from MSG SEVIRI. PET propagates forward in time and space the last available RR maps obtained from Advanced Microwave Sounding Unit (AMSU) and Microwave Humidity Sounder (MHS) observations by tracking BT of water vapor (6.2 μm) and thermal IR (10.8 μm) channels measured from the SEVIRI radiometer. PET is an iterative algorithm that exploits two separate modules, called Morphing and Calibration, in order to produce a new RR map for each step. The Morphing module modifies the shape and the position of the precipitating cells by applying a multithreshold and multiscale pattern analysis to the difference between IR and WV SEVIRI channels ($\Delta BT^{10.8\,\mu m-6.2\,\mu m}$), which is useful to detect the convective areas (Mosher 2001, 2002). Specifically, it maximizes the correlation index and minimizes the difference of two consecutive $\Delta BT^{10.8\,\mu m-6.2\,\mu m}$ related to many subregions to obtain an RR-morphed map. The Calibration module computes the $\Delta BT^{10.8\,\mu m-6.2\,\mu m}$–RR lookup table (LUT) by using the probabilistic histogram matching relationship (Calheiros and Zawadzki 1987) applied to the latest coincident $\Delta BT^{10.8\,\mu m-6.2\,\mu m}$ and RR values to obtain an RR-calibrated map. This module is able to estimate the increasing or decreasing stage of the cell size, as well as its genesis or extinction. RR-morphed and RR-calibrated maps are complementary, and the final RR map is obtained by their linear combination

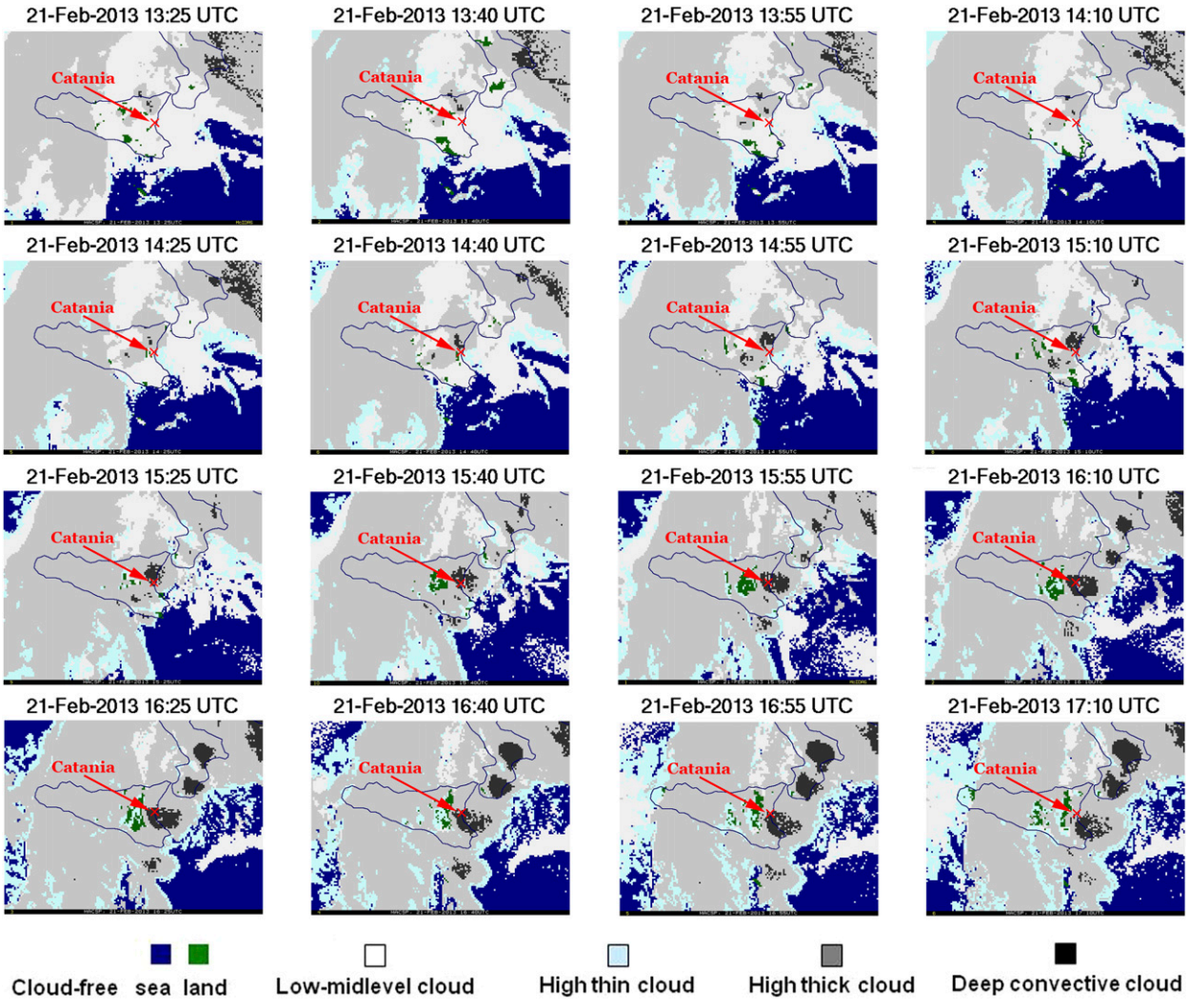

FIG. 3. Sequence of MACSP classification results from 1325 to 1710 UTC 21 Feb 2013.

computed pixel by pixel by evaluating the goodness of the Morphing procedure.

The PET algorithm exploits the high spatial and temporal sampling of GEO observations to fill the gap between two consecutive LEO overpasses. For this purpose, it starts with the latest available RR obtained using AMSU data and produces an RR map in the same grid of the SEVIRI radiometer for each step; this RR map is used for the following iterations until a new AMSU-based RR map is available.

In this paper, to start the PET algorithm, we use the RR field obtained by the PM–RR retrieval algorithm developed at IMAA-CNR, called Precipitation Estimation at Microwave Frequencies (PEMW; Di Tomaso et al. 2009), applied to the MHS overpass at 1315 UTC 21 February 2013. This was the latest PM observation available before the heavy rainfall occurred between 1500 and 1600 UTC. Figure 4 shows the RR map estimated by PEMW and the corresponding BT at 89 GHz from the MHS radiometer. Note that there is only low precipitation near Catania about 3 h before the main event.

Figure 5 shows the evolution of the precipitation field every 15 min, from 1325 to 1710 UTC, as estimated by the PET algorithm on the native SEVIRI grid. PET RR evolution starts after the last MHS overpass at 1315 UTC until 1710 UTC, when the most intense rainfall near Catania ended. The top left, corresponding to 1325 UTC, shows light precipitation, similarly to the PEMW estimates in Fig. 4 from which PET starts its propagation. The following five time steps in Fig. 5, between 1340 and 1440 UTC, show a small precipitation cell, with a maximum RR of about 5 mm h^{-1}, moving southeastward

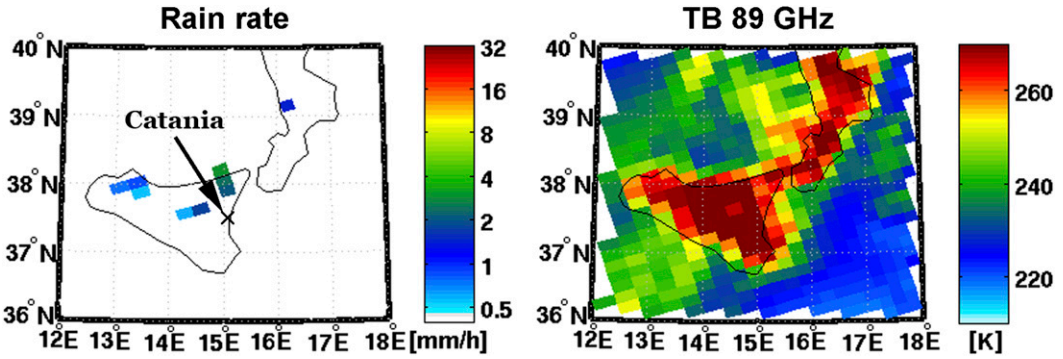

FIG. 4. (left) RR map with (right) the corresponding BT 89 GHz from MHS radiometer onboard the *NOAA-19* satellite at 1315 UTC 21 Feb 2013.

toward Catania but without any significant variations in size or intensity. In the next six time steps of Fig. 5, between 1455 and 1610 UTC, the precipitation cell over Catania expands quickly and its intensity increases up to more than 30 mm h^{-1}, with a peak larger than 50 mm h^{-1}, and with the contemporaneous formation of two new cells over the Calabria region. In this time interval, the total amount of precipitated rain over Catania

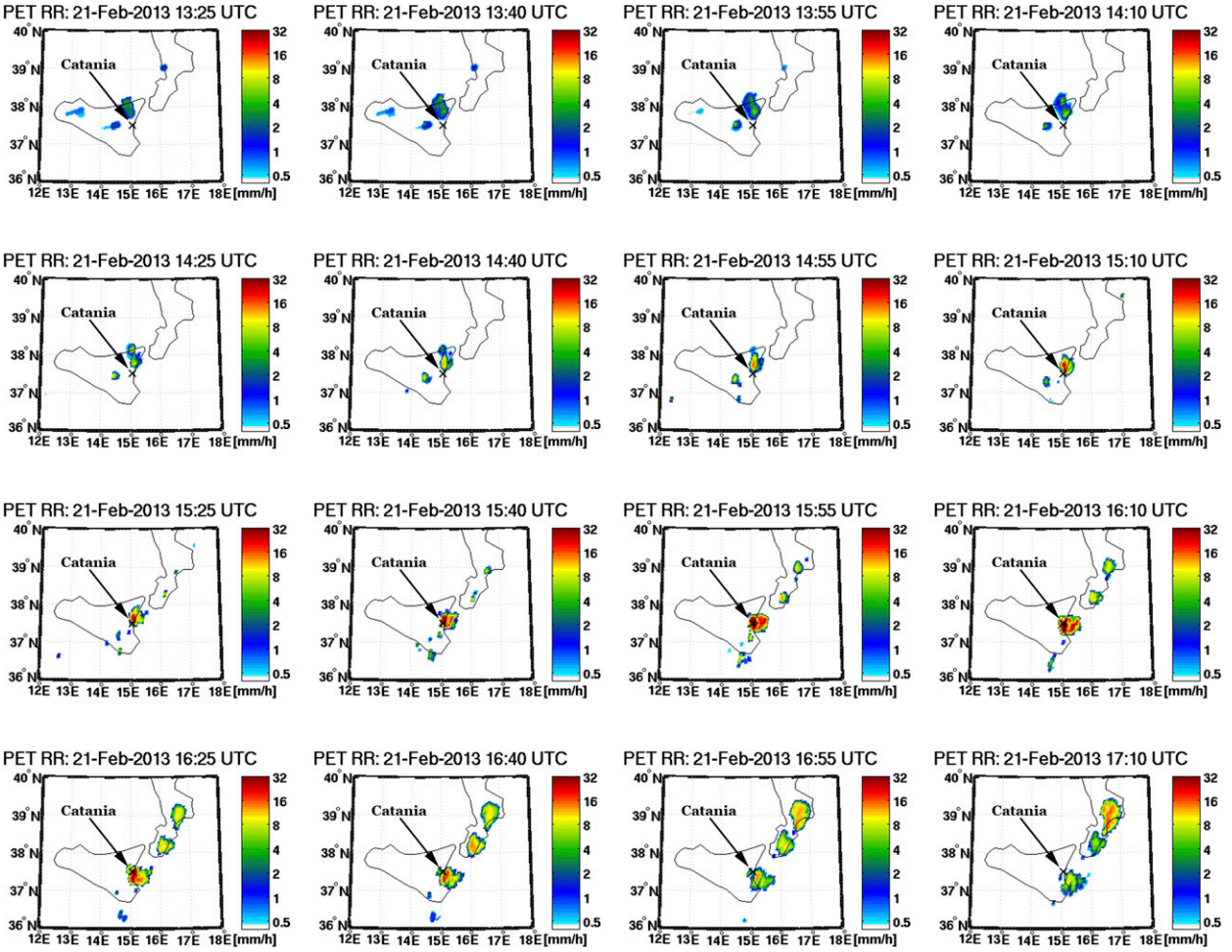

FIG. 5. PET RR maps from 1325 to 1710 UTC 21 Feb 2013.

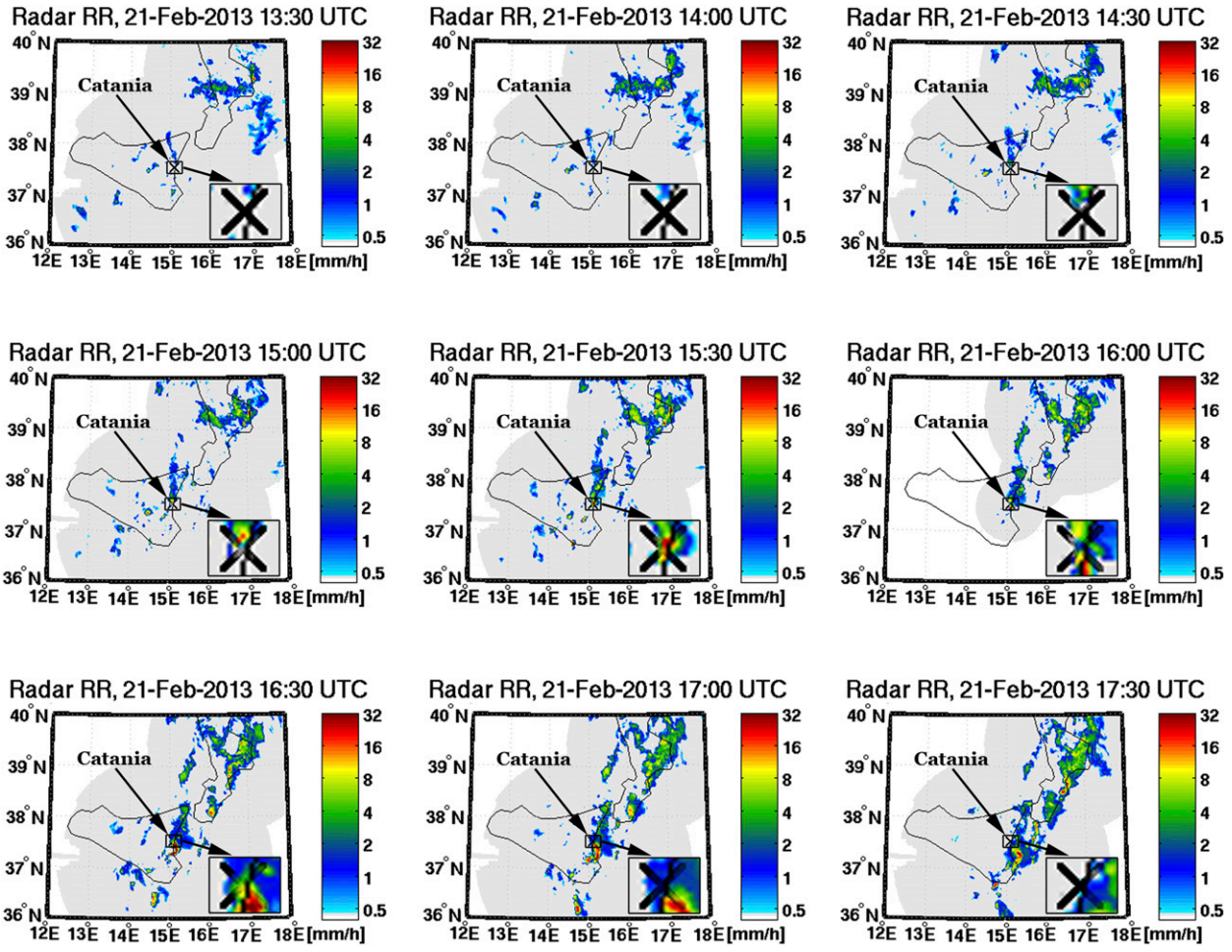

FIG. 6. RR maps from 1330 to 1730 UTC 21 Feb 2013 derived from Italian weather radar network.

reaches about 50 mm, causing the devastating flash flood in the city. In the last four time steps of Fig. 5, between 1625 and 1710 UTC, one can observe a progressive decrease in intensity and a movement southward of the main precipitation cell as well as a moderate variation of the other two cells.

The strong increase of the precipitation area and RR values obtained starting from the light precipitation over a small area given by PM–RR is caused by the Calibration module that expands the precipitating cell area and intensity on the basis of the $\Delta BT^{10.8\,\mu m-6.2\,\mu m}$ evolution. The spatial resolution of the PET RR map, better than that of the PM–RR used to initialize PET, is a result of the Morphing module that progressively arranges the starting precipitation on the SEVIRI grid.

5. Results evaluation

Figure 6 shows the evolution of the precipitation field every 30 min, from 1330 to 1730 UTC, as estimated by the weather radar network operated by the Italian DPC. The RR maps from 1330 to 1600 UTC show the formation and the movement of a small but strong precipitating cell exactly over Catania, with RR values up to 40 mm h^{-1}. The last time steps of Fig. 6, corresponding to the time interval from 1630 to 1730 UTC, show a progressive increase of the intense precipitating cell with a contemporary southward movement. This evolution is consistent with that shown by the MACSP sequence in Fig. 3, where a deep convective cell appears over Catania followed by two other cells over the Calabria region. By comparing the radar and the PET RR sequences, the maps show similar precipitating patterns and similar RR values, although the precipitation values differ pixel by pixel. The differences between the dimensions of the most intense cells as well as the difference between the maximum RR values of PET and radar over Catania, which are ~50 and ~40 mm h^{-1}, respectively, should be a consequence either of PET overestimation or radar underestimation.

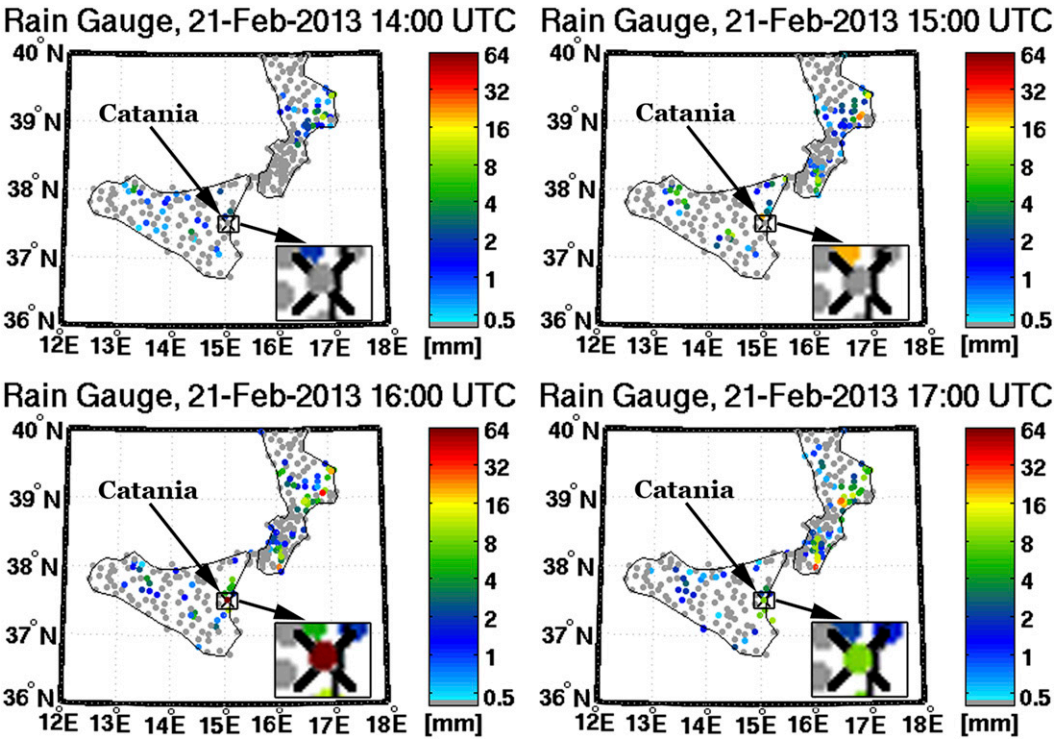

FIG. 7. The 1-h accumulated precipitation from 1400 to 1700 UTC 21 Feb 2013 derived from the Italian rain gauge network.

The latter hypothesis could be supported by Fig. 7, where the 1-h accumulated rain measured from the rain gauge network operated by the Italian DPC is shown. This figure shows that the evolution of the proposed case study agrees with the analysis carried out by MACSP and PET. In particular, the accumulated rainfall from 1500 to 1600 UTC, about 60 mm exactly over Catania, shows that PET correctly indicates the precipitation values.

Although a complete comparison between radar, rain gauge, MACSP, and PET is not possible in this context because many case studies would be needed for a reliable statistic, both radar and rain gauge measurements indicate an overall agreement with PET and MACSP estimates.

6. Summary and conclusions

The flash flood that hit Catania on 21 February 2013 was a consequence of heavy rainfall caused by a WCB originating from a depression that developed in northern Africa and moved across the Mediterranean Sea. The low frequency of severe storms for the winter season in the Mediterranean region as well as the rapid evolution of the rain cells and their small dimensions caused the absence of an adequate QPF of NWP model output. Similar misses are not rare and also occur for different meteorological situations, especially in summer when the convective events are frequent.

In this context, the satellite monitoring is particularly attractive for real-time operational purposes. For this reason, two different algorithms, MACSP and PET, based on satellite observations have been applied to the case study proposed. The former uses VIS and IR channels from SEVIRI to provide cloud classification maps, and the latter uses IR channels from SEVIRI coupled with rain rate obtained from MW-based algorithm to provide RR maps. While MACSP is able to produce cloud classification maps every 15 min, continuously and on the full Earth disk at native SEVIRI grid, PET produces RR maps every 15 min, for only a few hours after the last available PM observations and only on the region around the radiometer swath observations. On the other hand, MACSP can detect the convective areas without any quantitative information while PET yields an RR quantitative estimation. MACSP and PET are complementary for near-real-time weather condition monitoring, because when the latter is available, the former gives further information about cloud cover. In addition MACSP can be used also for the detection of convective areas.

For these reasons, both algorithms are very useful for real-time monitoring purposes, especially when NWP

QPF fails. Obviously, MACSP and PET cannot replace NWP models, but on the other hand, they can contribute in observing severe weather when convective events are not correctly forecast. Since quantitative precipitation forecasts by NWP may miss cases like in Catania, tools like MACSP and PET shall be adopted by civil protection centers in aid to the severe weather warning service.

Acknowledgments. The authors acknowledge the Italian Department of Civil Protection for providing data from the national radar network and the rain gauge network in the framework of the CETEMPS-DPC IDRA project. The authors are grateful to Valentina Colaiuda (CETEMPS) and Gianfranco Vulpiani (DPC) for helping with the interpretation of rain gauge and radar data, respectively.

REFERENCES

Adler, R. F., and R. A. Mack, 1984: Thunderstorm cloud height–rainfall rate relations for use with satellite rainfall estimation techniques. *J. Climate Appl. Meteor.,* **23,** 280–296, doi:10.1175/1520-0450(1984)023<0280:TCHRRF>2.0.CO;2.

——, and A. J. Negri, 1988: A satellite infrared technique to estimate tropical convective and stratiform rainfall. *J. Appl. Meteor.,* **27,** 30–51, doi:10.1175/1520-0450(1988)027<0030:ASITTE>2.0.CO;2.

——, M. J. Markus, and D. D. Fenn, 1985: Detection of severe Midwest thunderstorms using geosynchronous satellite data. *Mon. Wea. Rev.,* **113,** 769–781, doi:10.1175/1520-0493(1985)113<0769:DOSMTU>2.0.CO;2.

——, A. J. Negri, P. R. Keehn, and I. M. Hakkarinen, 1993: Estimation of monthly rainfall over Japan and surrounding waters from a combination of low-orbit microwave and geosynchronous IR data. *J. Appl. Meteor.,* **32,** 335–356, doi:10.1175/1520-0450(1993)032<0335:EOMROJ>2.0.CO;2.

Bennartz, R., and M. Schroeder, 2012: Convective activity over Africa and the tropical Atlantic inferred from 20 years of geostationary Meteosat infrared observations. *J. Climate,* **25,** 156–169, doi:10.1175/2011JCLI3984.1.

Bollettino di Vigilanza Meteorologica Nazionale, 2013, Bollettino di Vigilanza Meteorologica Nazionale del 21 febbraio 2013. [Available online at www.protezionecivile.gov.it/jcms/it/view_bvg.wp?contentId=BVG37845.]

Calheiros, R. V., and I. Zawadzki, 1987: Reflectivity–rain rate relationships for radar hydrology in Brazil. *J. Climate Appl. Meteor.,* **26,** 118–132, doi:10.1175/1520-0450(1987)026<0118:RRRRFR>2.0.CO;2.

Casella, D., S. Dietrich, F. Di Paola, M. Formenton, A. Mugnai, F. Porcù, and P. Sanò, 2012: PM-GCD—A combined IR–MW satellite technique for frequent retrieval of heavy precipitation. *Nat. Hazards Earth Syst. Sci.,* **12,** 231–240, doi:10.5194/nhess-12-231-2012.

——, and Coauthors, 2013: Transitioning from CRD to CDRD in Bayesian retrieval of rainfall from satellite passive microwave measurements: Part 2. Overcoming database profile selection ambiguity by consideration of meteorological control on microphysics. *IEEE Trans. Geosci. Remote Sens.,* **51,** 4650–4671, doi:10.1109/TGRS.2013.2258161.

Chen, F. W., and D. H. Staelin, 2003: AIRS/AMSU/HSB precipitation estimates. *IEEE Trans. Geosci. Remote Sens.,* **41,** 410–417, doi:10.1109/TGRS.2002.808322.

Cuo, L., and T. Pagano, 2011: A review of quantitative precipitation forecasts and their use in short- to medium-range streamflow forecasting. *J. Hydrometeor.,* **12,** 713–728, doi:10.1175/2011JHM1347.1.

Damrath, U., G. Doms, D. Fruhwald, E. Heise, B. Richter, and J. Steppeler, 2000: Operational quantitative precipitation forecasting at the German Weather Service. *J. Hydrol.,* **239,** 260–285, doi:10.1016/S0022-1694(00)00353-X.

Dietrich, S., D. Casella, F. Di Paola, M. Formenton, A. Mugnai, and P. Sanò, 2011: Lightning-based propagation of convective rain fields. *Nat. Hazards Earth Syst. Sci.,* **11,** 1571–1581, doi:10.5194/nhess-11-1571-2011.

Di Paola, F., and S. Dietrich, 2008: Resolution enhancement for microwave-based atmospheric sounding from geostationary orbits. *Radio Sci.,* **43,** RS6001, doi:10.1029/2007RS003789.

——, D. Casella, S. Dietrich, A. Mugnai, E. Ricciardelli, F. Romano, and P. Sanò, 2012: Combined MW-IR Precipitation Evolving Technique (PET) of convective rain fields. *Nat. Hazards Earth Syst. Sci.,* **12,** 3557–3570, doi:10.5194/nhess-12-3557-2012.

Di Tomaso, E., F. Romano, and V. Cuomo, 2009: Rainfall estimation from satellite passive microwave observations in the range 89 GHz to 190 GHz. *J. Geophys. Res.,* **114,** D18203, doi:10.1029/2009JD011746.

Ferraro, R. R., and Coauthors, 2005: NOAA operational hydrological products derived from the Advanced Microwave Sounding Unit. *IEEE Trans. Geosci. Remote Sens.,* **43,** 1036–1049, doi:10.1109/TGRS.2004.843249.

Gaudet, B., and W. R. Cotton, 1998: Statistical characteristics of a real-time precipitation forecasting model. *Wea. Forecasting,* **13,** 966–982, doi:10.1175/1520-0434(1998)013<0966:SCOART>2.0.CO;2.

Habets, F., P. LeMoigne, and J. Noilhan, 2004: On the utility of operational precipitation forecasts to served as input for streamflow forecasting. *J. Hydrol.,* **293,** 270–288, doi:10.1016/j.jhydrol.2004.02.004.

Hsu, K., X. Gao, S. Sorooshian, and H. V. Gupta, 1997: Precipitation estimation from remotely sensed information using artificial neural networks. *J. Appl. Meteor.,* **36,** 1176–1190, doi:10.1175/1520-0450(1997)036<1176:PEFRSI>2.0.CO;2.

Huffman, G. J., R. F. Adler, S. Curtis, D. T. Bolvin, and E. J. Nelkin, 2007: Global rainfall analyses at monthly and 3-h time scales. *Measuring Precipitation from Space: EURAINSAT and the Future,* V. Levizzani, P. Bauer, and F. J. Turk, Eds., Advances in Global Change Research, Vol. 28, Springer, 291–305.

Joyce, R. J., J. E. Janowiak, P. A. Arkin, and P. Xie, 2004: CMORPH: A method that produces global precipitation estimates from passive microwave and infrared data at high spatial and temporal resolution. *J. Hydrometeor.,* **5,** 487–503, doi:10.1175/1525-7541(2004)005<0487:CAMTPG>2.0.CO;2.

——, ——, P. Xie, and P. A. Arkin, 2007: CPC MORPHING technique (CMORPH). *Measuring Precipitation from Space: EURAINSAT and the Future,* V. Levizzani, P. Bauer, and F. J. Turk, Eds., Advances in Global Change Research, Vol. 28, Springer, 307–317.

Kidd, C., and V. Levizzani, 2011: Status of satellite precipitation retrievals. *Hydrol. Earth Syst. Sci.,* **15,** 1109–1116, doi:10.5194/hess-15-1109-2011.

——, D. R. Kniveton, M. C. Todd, and T. J. Bellerby, 2003: Satellite rainfall estimation using combined passive microwave and infrared algorithms. *J. Hydrometeor.,* **4,** 1088–1104, doi:10.1175/1525-7541(2003)004<1088:SREUCP>2.0.CO;2.

——, F. J. Tapiador, V. Sanderson, and D. Kniveton, 2007: The University of Birmingham global rainfall algorithms. *Measuring Precipitation from Space: EURAINSAT and the Future,* V. Levizzani, P. Bauer, and F. J. Turk, Eds., Advances in Global Change Research, Vol. 28, Springer, 255–267.

Kubota, T., and Coauthors, 2007: Global precipitation map using satellite-borne microwave radiometers by the GSMaP project: Production and validation. *IEEE Trans. Geosci. Remote Sens.,* **45,** 2259–2275, doi:10.1109/TGRS.2007.895337.

Kucera P. A., E. E. Ebert, F. J. Turk, V. Levizzani, D. Kirschbaum, F. J. Tapiador, A. Loew, and M. Borsche, 2013: Precipitation from space: Advancing Earth system science, *Bull. Amer. Meteor. Soc.,* **94,** 365–375, doi:10.1175/BAMS-D-11-00171.1.

Kummerow, C. D., and Coauthors, 2001: The evolution of the Goddard profiling algorithm (GPROF) for rainfall estimation from passive microwave sensors. *J. Appl. Meteor.,* **40,** 1801–1820, doi:10.1175/1520-0450(2001)040<1801:TEOTGP>2.0.CO;2.

——, S. Ringerud, J. Crook, D. Randel, and W. Berg, 2010: An observationally generated a priori database for microwave rainfall retrievals. *J. Atmos. Oceanic Technol.,* **28,** 113–130, doi:10.1175/2010JTECHA1468.1.

Lensky, I. M., and D. Rosenfeld, 2008: Clouds–Aerosols–Precipitation Satellite Analysis Tool (CAPSAT). *Atmos. Chem. Phys.,* **8,** 6739–6753, doi:10.5194/acp-8-6739-2008.

Marzano, F. S., M. Palmacci, D. Cimini, G. Giuliani, and J. F. Turk, 2004: Multivariate statistical integration of satellite infrared and microwave radiometric measurements for rainfall retrieval at the geostationary scale. *IEEE Trans. Geosci. Remote Sens.,* **42,** 1018–1032, doi:10.1109/TGRS.2003.820312.

Meneguzzo, F., M. Pasqui, G. Menduni, G. Messeri, B. Gozzini, D. Grifoni, M. Rossi, and G. Maracchi, 2004: Sensitivity of meteorological high-resolution numerical simulations of the biggest floods occurred over the Arno river basin, Italy, in the 20th century. *J. Hydrol.,* **288,** 37–56, doi:10.1016/j.jhydrol.2003.11.032.

Mosher, F. R., 2001: A satellite diagnostic of global convention, Preprints, *11th Conf. on Satellite Meteorology,* Madison, WI, Amer. Meteor. Soc., 416–419.

——, 2002: Detection of deep convection around the globe, Preprints, *10th Conf. on Aviation, Range, and Aerospace Meteorology,* Portland, OR, Amer. Meteor. Soc., 1.7. [Available online at https://ams.confex.com/ams/pdfpapers/38600.pdf.]

Mugnai, A., and Coauthors, 2013a: CDRD and PNPR satellite passive microwave precipitation retrieval algorithms: EuroTRMM/EURAINSAT origins and H-SAF operations. *Nat. Hazards Earth Syst. Sci.,* **13,** 887–912, doi:10.5194/nhess-13-887-2013.

——, and Coauthors, 2013b: Precipitation products from the hydrology SAF. *Nat. Hazards Earth Syst. Sci.,* **13,** 1959–1981, doi:10.5194/nhess-13-1959-2013.

Munchak, S. J., and G. Skofronick-Jackson, 2013: Evaluation of precipitation detection over various surfaces from passive microwave imagers and sounders. *Atmos. Res.,* **131,** 81–94, doi:10.1016/j.atmosres.2012.10.011.

Negri, A. J., and R. F. Adler, 1981: Relation of satellite based thunderstorm intensity to radar estimated rainfall. *J. Appl. Meteor.,* **20,** 288–300, doi:10.1175/1520-0450(1981)020<0288:ROSBTI>2.0.CO;2.

Price, C., and Coauthors, 2011: Using lightning data to better understand and predict flash floods in the Mediterranean. *Surv. Geophys.,* **32,** 733–751, doi:10.1007/s10712-011-9146-y.

Ricciardelli, E., F. Romano, and V. Cuomo, 2008: Physical and statistical approaches for cloud identification using Meteosat Second Generation-Spinning Enhanced Visible and Infrared Imager. *Remote Sens. Environ.,* **112,** 2741–2760, doi:10.1016/j.rse.2008.01.015.

Shrestha, D. L., D. E. Robertson, Q. J. Wang, T. C. Pagano, and P. Hapuarachchi, 2013: Evaluation of numerical weather prediction model precipitation forecasts for short-term streamflow forecasting purpose. *Hydrol. Earth Syst. Sci.,* **17,** 1913–2013, doi:10.5194/hess-17-1913-2013.

Sorooshian, S., K. Hsu, X. Gao, H. V. Gupta, B. Imam, and D. Braithwaite, 2000: Evaluation of PERSIANN system satellite-based estimates of tropical rainfall. *Bull. Amer. Meteor. Soc.,* **81,** 2035–2046, doi:10.1175/1520-0477(2000)081<2035:EOPSSE>2.3.CO;2.

Surussavadee, C., and D. H. Staelin, 2008: Global millimeter-wave precipitation retrievals trained with a cloud-resolving numerical weather prediction model, Part I: Retrieval design. *IEEE Trans. Geosci. Remote Sens.,* **46,** 99–108, doi:10.1109/TGRS.2007.908302.

Torricella, F., V. Levizzani, and F. J. Turk, 2007: Application of a blended MW-IR rainfall algorithm to the Mediterranean. *Measuring Precipitation from Space: EURAINSAT and the Future,* V. Levizzani, P. Bauer, and F. J. Turk, Eds., Advances in Global Change Research, Vol. 28, Springer, 497–507.

Turk, F. J., and A. V. Mehta, 2007: Towards improvements in short time scale satellite-derived precipitation estimates using blended satellite techniques. *Measuring Precipitation from Space: EURAINSAT and the Future,* V. Levizzani, P. Bauer, and F. J. Turk, Eds., Advances in Global Change Research, Vol. 28, Springer, 281–290.

Wardah, T., S. H. Abu Bakar, A. Bardossy, and M. Maznorizan, 2008: Use of geostationary meteorological satellite images in convective rain estimation for flash-flood forecasting. *J. Hydrol.,* **356,** 283–298, doi:10.1016/j.jhydrol.2008.04.015.

——, A. A. Kamil, A. B. Sahol Hamid, and W. W. I. Maisarah, 2011: Quantitative precipitation forecast using MM5 and WRF models for Kelantan River basin. *Int. J. Environ. Earth Sci. Eng.,* **5,** 36–40.

Wilcox, E. M., and L. J. Donner, 2007: The frequency of extreme rain events in satellite rain-rate estimates and an atmospheric general circulation model. *J. Climate,* **20,** 53–69, doi:10.1175/JCLI3987.1.

Wu, H., R. F. Adler, Y. Hong, Y. Tian, and F. Policelli, 2012: Evaluation of global flood detection using satellite-based rainfall and a hydrologic model. *J. Hydrometeor.,* **13,** 1268–1284, doi:10.1175/JHM-D-11-087.1.

Wu, R., J. A. Weinman, and R. T. Chin, 1985: Determination of rainfall rates from GOES satellite images by a pattern recognition technique. *J. Atmos. Oceanic Technol.,* **2,** 314–330, doi:10.1175/1520-0426(1985)002<0314:DORRFG>2.0.CO;2.

Zimmer, M., and H. Wernli, 2011: Verification of quantitative precipitation forecasts on short time-scales: A fuzzy approach to handle timing errors with SAL. *Meteor. Z.,* **20,** 95–105, doi:10.1127/0941-2948/2011/0224.